Spatial mapping of the internal and external electromagnetic fields of negative index metamaterials

Bryan J. Justice, Jack J. Mock, Liheng Guo, Aloyse Degiron, David Schurig, and David R. Smith

Department of Electrical and Computer Engineering, Duke University, Durham, NC 27708 USA
drsmith@ee.duke.edu
http://www.ee.duke.edu/~drsmith

Abstract: We perform an experimental study of the phase and amplitude of microwaves interacting with and scattered by two-dimensional negative index metamaterials. The measurements are performed in a parallel plate waveguide apparatus at X-band frequencies (8-12 GHz), thus constraining the electromagnetic fields to two dimensions. A detection antenna is fixed to one of the plates, while a second plate with a fixed source antenna or waveguide is translated relative to the first plate. The detection antenna is inserted into, but not protruding below, the stationary plate so that fields internal to the metamaterial samples can be mapped. From the measured mappings of the electric field, the interplay between the microstructure of the metamaterial lattice and the macroscopic averaged response is revealed. For example, the mapped phase fronts within a metamaterial having a negative refractive index are consistent with a macroscopic phase—in accordance with the effective medium predictions—which travels in a direction opposite to the direction of propagation. The field maps are in excellent agreement with finite element numerical simulations performed assuming homogeneous metamaterial structures.

OCIS codes: (260.0260) Physical optics; (080.0080) Geometrical optics

References and links

1. R. M. Walser, "Electromagnetic metamaterials," in *Complex Mediums II: Beyond Linear Isotropic Dielectrics,* A. Lakhtakia, W. S. Weiglhofer, I. J. Hodgkinson, eds., Proc. SPIE **4467**, 1-15 (2001).
2. D. R. Smith, J. B. Pendry, and M. C. K. Wiltshire, "Metamaterials and negative refractive index," Science **305**, 788-792 (2004).
3. Z. G. Dong, S. N. Zhu, H. Liu, J. Zhu, and W. Cao, "Numerical simulations of negative-index refraction in wedge-shaped samples," Phys. Rev. E **72**, 016607 (2005).
4. D. R. Smith, S. Schultz, P. Markoš and C. M Soukoulis, "Determination of effective permittivity and permeability of metamaterials from reflection and transmission coefficients," Phys. Rev. B **65**, 195104 (2002).
5. X. D. Chen, T. M. Grzegorczyk, B. I. Wu, J. Pacheco, and J. A. Kong, "Robust method to retrieve the constitutive effective parameters of metamaterials," Phys. Rev. E **70**, 016608 (2004).
6. D. R. Smith and J. B. Pendry, "Homogenization of metamaterials by field averaging," J. Opt. Soc. Am. B **23**, 391-403 (2006).
7. T. Koschny, P. Markoš, D. R. Smith, and C. M. Soukoulis, "Resonant and antiresonant frequency dependence of the effective medium parameters of metamaterials," Phys. Rev. E **68**, 065602 (2003).
8. T. Koschny, P. Markoš, E. N. Economou, D. R. Smith, D. C. Vier, and C. M. Soukoulis, "Impact of inherent periodic structure on effective medium description of left-handed and related metamaterials," Phys. Rev. B **71**, 245105 (2005).
9. D. R. Smith, Willie J. Padilla, D. C. Vier, S. C. Nemat-Nasser, and S. Schultz, "A composite medium with simultaneously negative permeability and permittivity," Phys. Rev. Lett. **84,** 4184-4187 (2000).

#73265 - $15.00 USD Received 21 July 2006; revised 6 September 2006; accepted 6 September 2006

10. R. Shelby, D. R. Smith, and S. Schultz, "Experimental verification of a negative index of refraction," Science **292**, 77-79 (2001).
11. C. G. Parazzoli, R. B. Greegor, K. Li, B. E. C. Koltenbah and M. Tanielian, "Experimental verification and simulation of negative index of refraction using Snell's law," Phys. Rev. Lett. **90** 107401 (2002).
12. A. A. Houck, J. B. Brock and I. L. Chuang, "Experimental observations of a left-handed material that obeys Snell's law," Phys. Rev. Lett. **90**, 137401 (2003).
13. R. W. Ziolkowski, "Design, fabrication and testing of double negative metamaterials," IEEE Trans. Antennas Propag. **51**, 1516-1529 (2003).
14. R. B. Greegor, C. G. Parazzoli, K. Li, B. E. C. Koltenbah and M. Tanielian, "Experimental determination and numerical simulation of the properties of negative index of refraction metamaterials," Opt. Express **11**, 688-695 (2003).
15. C. G. Parazzoli, R. B. Greegor, J. A. Nielsen, M. A. Thompson, K. Li, A. M. Vetter, M. H. Tanielian, and D. C. Vier, "Performance of a negative index of refraction lens," Appl. Phys. Lett. **84**, 3232-3234 (2004).
16. R. B. Greegor, C. G. Parazzoli, J. A. Nielsen, M. A. Thompson, M. H. Tanielian, and D. R. Smith, "Simulation and testing of a graded negative index of refraction lens," Appl. Phys. Lett. **87**, 091114 (2005).
17. T. Driscoll, D. N. Basov, A. F. Starr, P. M. Rye, S. Nemat-Nasser, D. Schurig, and D. R. Smith, "Free-space microwave focusing by a negative-index gradient lens," Appl. Phys. Lett. **88**, 081101 (2006).
18. B. I. Popa and S. A. Cummer, "Wave fields measured inside a negative refractive index metamaterial," Appl. Phys. Lett. **85**, 4564-4566 (2004).
19. B. I. Popa and S. A. Cummer, "Direct measurement of evanescent wave enhancement inside passive metamaterials," Phys. Rev. E **73**, 016617 (2006).
20. J. B. Pendry, D. Schurig, and D. R. Smith, "Controlling electromagnetic fields," Science **312**, 1780-1782 (2006).
21. U. Leonhardt, "Optical conformal mapping," Science **312**, 1777-1780 (2006).
22. D. R. Smith, D. Schurig, J. J. Mock, P. Kolinko, and P. Rye, "Partial focusing of radiation by a slab of indefinite media," Appl. Phys. Lett. **84**, 2244-2246 (2004).
23. P. V. Parimi, W. T. Lu, P. Vodo, J. Sokoloff, J. S. Derov, and S. Sridhar, "Negative refraction and left-handed electromagnetism in microwave photonic crystals," Phys. Rev. Lett. **92**, 127401 (2004).
24. P. Vodo, P. V. Parimi, W. T. Lu, and S. Sridhar, "Focusing by planoconcave lens using negative refraction," Appl. Phys. Lett. **86**, 201108 (2005).
25. D. R. Smith, P. Kolinko, and D. Schurig, "Negative refraction in indefinite media," J. Opt. Soc. Am. B **21**, 1032-1043 (2004).
26. C. P. Parazzoli and K. Li, Phantom Works, The Boeing Company (personal communication, 2005).
27. V. G. Veselago "The electrodynamics of substances with simultaneously negative values of ε and μ," Soviet Physics USPEKI **10**, 509-514 (1968).
28. J. N. Gollub, D. R. Smith, D. C. Vier, T. Perram, and J. J. Mock, "Experimental characterization of magnetic surface plasmons on metamaterials with negative permeability," Phys. Rev. B **71**, 195402 (2005).
29. P. Kolinko and D. R. Smith, "Numerical study of electromagnetic waves interacting with negative index materials," Opt. Express **11**, 640-648 (2003).
30. D. R. Smith, P. M. Rye, J. J. Mock, D. C. Vier, and A. F. Starr, "Enhanced diffraction from a grating on the surface of a negative-index metamaterial," Phys. Rev. Lett. **93**, 137405 (2004).

1. Introduction

Metamaterials have brought about a new perspective to the field of electromagnetism [1, 2]. Underlying the metamaterials approach is the concept that a periodic arrangement of scattering elements can be treated to good approximation as a homogeneous material, characterized by bulk parameters such as the electric permittivity, ε, and the magnetic permeability, μ. ε and μ are "macroscopic" parameters, in the sense that they represent an averaging over the "microscopic"—or sub-wavelength—structure of the inhomogeneous composite. An indicator of the validity of the metamaterials approach is the degree to which the scattering behavior of metamaterial structures can be predicted solely by substituting the expected or retrieved macroscopic values of ε and μ in place of the microscopic metamaterial structure.

For metamaterials based on periodically repeated elements, the properties of the bulk composite can be derived from consideration of the properties of just one of the repeated unit cells of the material. This simplification enables a two-step process for metamaterial design. In what is a typical design cycle, a homogeneous medium with desired electromagnetic properties (i.e., ε and μ) is simulated in the context of a device or application, with the electromagnetic material parameters of the medium fine-tuned as necessary by the

#73265 - $15.00 USD Received 21 July 2006; revised 6 September 2006; accepted 6 September 2006

optimization of the overall system performance. Then, a metamaterial can be designed by simulating and successively refining a single unit cell of an assumed periodic structure until the retrieved effective medium parameters match those desired. This design process obviates the need for explicit simulations that would require the discretization of possibly hundreds of micro-scale (subwavelength) unit cells in the computational domain, and represents a solution to what is a multiscale simulation problem. Although Dong *et al.* [3] have successfully demonstrated that such simulations are possible—simulating a negative index wedge comprising over one hundred individual metamaterial elements—still, large-scale simulations remain too time-consuming for routine optimization.

Over the past several years computational effective medium approaches have been developed and refined, in which the effective medium parameters for a metamaterial are retrieved from full-wave electromagnetic unit cell simulations [4-6]. Although there are often unusual artifacts and anomalies that occur in the retrieved parameters [7, 8], numerous experimental confirmations have shown that the retrieved parameters accurately describe the electromagnetic properties of the composite metamaterial structures [9-17]. For example, negative index and gradient index metamaterial lenses have been designed and constructed following the procedures described above, with their focusing and other lensing properties demonstrated to be in excellent agreement with predictions [15-17].

To date, the main method of confirmation of the properties of metamaterials has been to compare the measured transmission, reflection and other scattering properties with effective medium simulations. That is, the influence of a metamaterial sample on incident radiation is usually determined by measurement of the fields external to the sample. A notable exception has been the work by Popa *et al.* who have measured the amplitude and phase of the electric field *within* a metamaterial structure [18, 19]. To obtain these mappings, Popa *et al.* construct metamaterial samples designed to operate at microwave frequencies (2.6 GHz), and embed them within of a section of WR340 waveguide. A line of access holes drilled into the top of the waveguide allows a coaxial probe to be inserted into the waveguide region and to measure the local electric field along the central axis of the waveguide. Despite complications due to the fundamental mode being a waveguide mode (TE_{10}) rather than a free space mode (*TEM*), as well as the inherent one-dimensional nature of the configuration, the authors have successfully confirmed the negative phase advance characteristic of materials with negative refractive index [18], as well as the phenomenon of evanescent wave refocusing [19].

The results of Popa *et al.* demonstrate that a direct confirmation of the effective medium properties of a 1-D metamaterial can be determined by studying the fields within a metamaterial structure. The experimentally obtained results also indicate that a well defined macroscopic phase can be obtained that is relatively insensitive to the local micro-scale metamaterial structure.

In this paper, we extend the concept of point-by-point phase-sensitive field measurements to obtain spatial field maps of metamaterial samples within a two-dimensional planar waveguide apparatus. In these measurements, the electric field is sampled at intervals much finer than the dimension of the unit cell, thus providing unique information as to the interplay between the local microscopic properties and the averaged effective medium properties associated with actual fabricated metamaterials, which are in actuality far from homogenous. These field maps can provide a decisive confirmation of the validity of the effective medium description of a metamaterial, in addition to being a useful general tool for assessing the performance of artificially structured materials. For example, we will see that the homogeneous description of the metamaterial is actually approximate; local spatial regions within a given sample can be identified that have defects or whose properties differ significantly from the average. For these cases, field maps are a particularly useful diagnostic that provide a path to improve metamaterial performance. The field maps may be especially of value for metamaterials having complicated gradients in their material properties, such as the transformation media recently suggested [20, 21].

Planar waveguide mapping chambers have been used previously to study a variety of electromagnetic structures, including negative index lenses and prisms composed of

#73265 - $15.00 USD Received 21 July 2006; revised 6 September 2006; accepted 6 September 2006

metamaterials or photonic crystals [12, 15, 22-24]. In most of these prior works, however, only the field distribution external to the sample being measured was reported, although phase-sensitive measurements have been presented [23, 24]. In the field maps presented here, both the amplitude and phase of the internal fields of metamaterial samples are measured, allowing us to form an image that can be compared directly with numerical simulations. For the first time, we are able to measure directly the negative phase advance within a negative index metamaterial wedge, correlating the internal backward waves with the external negative refracted waves.

2. Experimental technique

The field mapping apparatus that we utilize is similar in concept to previously described versions [12, 15, 22-24]. By confining electromagnetic waves between two conducting planes, it is possible to reduce the microwave scattering to two dimensions, so long as only the lowest transverse electromagnetic (TEM) mode is excited. For this mode, the electric and magnetic fields do not vary along the axis between the plates (z-axis). Ideally, only structures that do not break translational symmetry along the z-axis can rigorously scatter only the TEM mode. In general, we expect that a less symmetric structure will couple also to a collection of higher order modes, characterized by fields that vary along the z-axis. However, by choosing frequencies such that these latter modes remain beyond cutoff, we expect the fields not associated with a TEM mode scattered from any of the metamaterial elements to be restricted to a very local region about the elements, and negligible when compared with the effective medium scattering of the composite. (The field maps presented here will illustrate the extent to which the local fields impact the homogeneous approximation.)

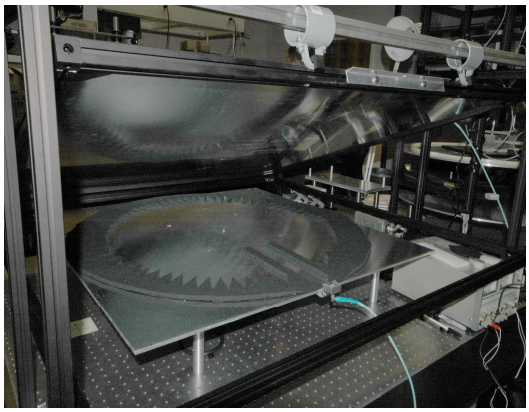

Fig. 1. Photograph of the field mapping planar waveguide chamber in the open position. The upper plate (including the detector antenna) is lowered parallel to the lower plate prior to the scan and after the sample is positioned relative to the source on the lower plate. The lower plate is mounted to two computer controlled linear translation stages, enabling an area of 20 cm by 20 cm to be scanned in steps of 1 mm (or less if desired). The detector probe mounted in the stationary upper plate can detect the amplitude and phase of the electric field within the chamber.

Since the electromagnetic fields are mostly invariant along the z-axis of the chamber, a map of the fields at any plane within the chamber should provide an equivalent characterization of the scattering. This equivalence is convenient, because it allows us to perform a map of the field *just above* the structure rather than inside, where it would be difficult to insert a probe antenna that would not also alter the field pattern. Throughout this paper, when we discuss field maps "within" a metamaterial or other sample, we will be referring to the field detected just *above* the sample.

#73265 - $15.00 USD Received 21 July 2006; revised 6 September 2006; accepted 6 September 2006

To obtain the field maps presented here, we assembled a planar waveguide chamber (Fig. 1) consisting of an upper and a lower aluminum plate made from ¼" tooled aluminum sheet. The upper plate is 4' x 4' and the lower plate is 3' x 3'. The overhang of the upper plate ensures that the same electromagnetic boundary conditions are maintained, even as the lower plate is translated. The upper plate is held in place using a frame built with 1" structural rails (ThorLabs, NJ). To obtain optimal mapping data, we found it necessary to rigidize the ¼" upper plate so as to remove any inherent sag. Aluminum bars are bolted to the upper plate and the tension of the bolts adjusted until the plate is flattened. Without straightening, the 4' x 4' upper plate exhibits a severe amount of sag that causes artifacts to be introduced into the field maps. The mapping area within the planar waveguide chamber is set by a ring of microwave absorber (R & F products, part# RFLS-35-.390) cut into a saw-toothed pattern roughly 5 cm thick and fixed to the lower plate. The absorber has an attenuation rate of 15dB/inch. The diameter of the ring of absorber is approximately 30" and serves to reduce reflections from the waveguide edges back into the mapping region.

All of the metamaterial structures presented here are designed to exhibit properties of interest at X-band frequencies (8-12 GHz). To fit between the plates without causing drag, the samples are designed to be 10 mm in height (along the z-axis), with the planar waveguide plate separation set to be 11 mm. The 11 mm spacing presumably lowers the cutoff frequencies for the higher order modes, but not significantly enough to impact the measurements reported here.

Either a planar beam or a radial wave can be excited by introducing microwaves into the chamber by an X-band waveguide adapter or a coaxial antenna (with the center pin extending into the chamber). In both cases, the source feeds are fixed to the lower plate, as is the metamaterial sample; in this way, the samples and the sources do not move relative to each other during the scan. The fields internal and external to samples in the chamber are detected by a coaxial antenna mounted onto the upper plate such that the center pin and the dielectric sheath are cut flush with the plate and do not extend into the chamber. In practice, we have found that with this configuration we can achieve reasonable signal-to-noise, in part due the large dynamic range of the Vector Network Analyzer (VNA) (Agilent, model number N5230A). Repeated scans over a source antenna inserted into the lower plate, with the detector center pin extending different lengths (from 1 cm to 0 cm) into the chamber, reproduced the exact same field patterns, although the overall signal level was reduced considerably as the pin length was reduced.

To achieve automated scanning, the bottom plate is attached to a pair of orthogonal XY computer controlled linear stages (Optosigma, product number SGSP33-200XY). The working scan range is 20 cm by 20 cm. The linear stages have a step resolution of ~100 μm, although the scans presented here were taken at a resolution of 1 mm between steps, resulting in field maps typically having 200 x 200 data points. The VNA provides the source microwave signal and phase sensitive detection of the return signal. A custom LabView program coordinates the motion of the stages and scan with the data acquisition of the VNA. The transmitted signal (S_{21}) data are stored as complex values in matrices that can be plotted as intensity maps using scripts written in MATLAB.

To assess the performance of the apparatus, two types of sources were studied in the absence of any scattering elements: a point source and a collimated beam. To introduce a point source for microwaves, a flexible coaxial cable (Micro-Coax, UFB197C) is attached to a brass, coaxial panel receptacle (Amphenol, 901-9891-RFX). The receptacle has a coaxial fitting on one side, and dielectric-clad center pin on the other. The receptacle is mounted on the outside of the upper plate, with the center pin protruding through a hole drilled into the chamber. Cylindrical waves are launched from the fitting when excited. Note that this form of excitation does not constitute an ideal line source due to the reflection boundary conditions at the top and bottom waveguide plates; however, because the antenna couples predominantly to the lowest order cylindrical propagating mode, we expect the experimentally mapped fields to be in agreement with the ideal line source, except on or within a wavelength of the fitting.

#73265 - $15.00 USD Received 21 July 2006; revised 6 September 2006; accepted 6 September 2006

Because of the translational invariance between the bounding plates, the electromagnetic modes of interest correspond to solutions of the two-dimensional scalar wave equation in which the electric field is polarized along the z-axis. Thus, we would expect the electric field distribution away from the antenna to correspond to the lowest order outgoing Hankel function, the real part of which is plotted in Fig. 2(a). To confirm this, we acquire both the real and imaginary parts of the electric field as a function of position $[E(x,y) = E_r(x,y) + iE_i(x,y)]$. The phase of the field at a given detection location is referenced to the output port of the VNA. This reference is arbitrary for our purposes, so that we are free to advance the phase of the acquired data scan when necessary to match up with analytical theory or simulations. An alternative and convenient means to visualize the complex field is to advance the arbitrary phase factor, φ, in equal steps through 360° and plot the real part of $E(x,y)\exp(i\varphi)$. Viewed as an animation, we are then able to picture the propagation characteristics of the field.

The real part of the measured electric field is shown in Fig. 2(b). We see that, away from the very central region, the measured and analytical field plots are nearly identical. Moreover, the corresponding animation of the measured fields reveals phase fronts that move outward from the source, as would be expected. Line scans of the Hankel function and the measured fields at 10 GHz, shown in Fig. 2(c), demonstrate the quite close agreement of the measured fields with the analytical description, as well as the excellent signal-to-noise ratio of the measurements.

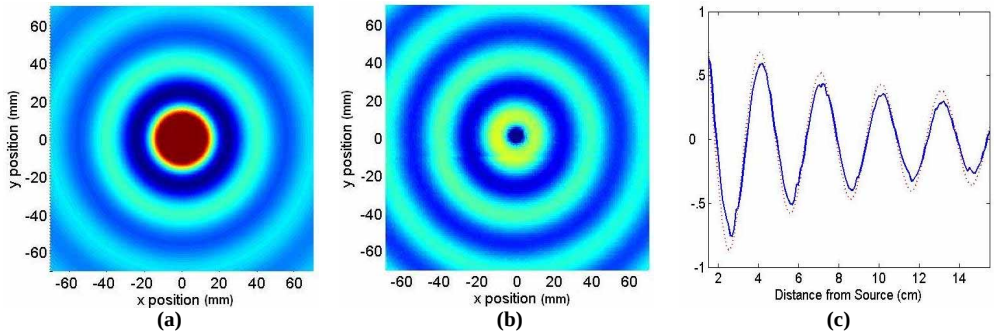

Fig. 2. (a). Field map of the real part of the lowest order outgoing Hankel function (scale in mm). (b) (1.65 MB) The measured real part of the electric field radiated by a coaxial antenna introduced into the lower plate of the planar waveguide apparatus (scale in mm). (c) A comparison of the line scans corresponding to the measured field (solid line) and the lowest order outgoing Hankel function (dashed line).

In principle, the excitation providing the most accessible interpretation for scattering experiments would be a plane wave; however, the finite aperture of any waveguide transition produces diffraction. Within the constraints of our chamber size and with a single, fixed source, our best approximation to the plane wave is to produce a minimally diverging, finite-width beam. We form a beam in the planar waveguide by taking the coaxial cable from the network analyzer and attaching it to a coaxial waveguide adapter (Advanced Technical Materials, part number 90-251A-6) that is fixed to the edge of the lower plate of the planar waveguide. So that the plates can still be moved relative to each other, the upper portion of the adapter has been milled away, allowing the upper plate to replace the top wall of the adapter. Away from the adapter, a guiding channel is formed using microwave absorbing material (see Fig. 1). Throughout the following experiments, channels of different widths were assembled, leading to varying diffraction-limited beams projected into the sample region. The intensity and the real part of the electric field corresponding to a typical beam are shown in Fig. 3. For this beam, the width of the channel was 9 cm and the length 30 cm. The

#73265 - $15.00 USD Received 21 July 2006; revised 6 September 2006; accepted 6 September 2006

amplitude of the beam is slightly peaked in the center, while the phase fronts reveal a gentle expansion as the wave emerges from the channel, as expected.

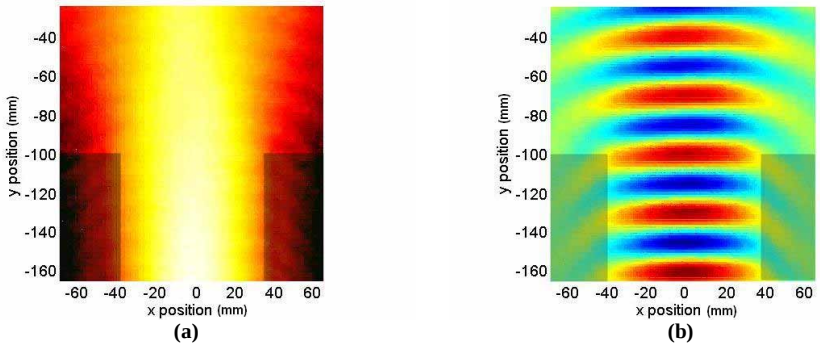

Fig. 3. (a). Measured spatial map of the intensity of the electric field corresponding to a planar beam generated within the planar waveguide. (b) (1.63 MB) Measured spatial map of the real part of the electric field field. The channel, made using absorbing material, is indicated by the lighter portions on the figures.

3. Positive index wedge experiments

The index-of-refraction is a property associated with a homogeneous material. One of the common techniques of measuring the refractive index of a material is to form the material into a wedge, such that a wave that illuminates one surface of the wedge is refracted at an angle as it emerges from the opposite surface of the wedge. In the far field, the observed angle of the emerging wave provides a measure of the refractive index of the wedge material through Snell's Law. For negative index metamaterials, this refraction experiment has served as an important diagnostic [10-12]; however, while the wedge experiment is conceptually simple, its application to the characterization of metamaterials is somewhat more complicated since metamaterials are inherently inhomogeneous. One of our goals in mapping the fields of artificially structured metamaterial samples is to ascertain whether the internal field distribution in a metamaterial sample behaves in the same manner as it would in a homogeneous material with equivalent electromagnetic properties.

To first test our ability to map the fields associated with a homogeneous material, we constructed a wedge out of a 10 mm thick polycarbonate (ε=2.6) sheet. As discussed above, since it is not possible to insert the probe into the material, the fields "within" the wedge are assumed to be proportional to the fields just above the wedge, where the fields can be detected. It can be expected that the impedance properties of the probe will be altered by the material properties of the sample, such that the permittivity or permeability of a given sample will enter as a factor into the detected signal. We do not attempt to calculate this effect here, as we are primarily concerned with the phase and overall propagation characteristics of the sample.

An example of the refraction of a beam from the polycarbonate wedge, taken at a frequency of 10.5 GHz, is shown in Fig. 4. The mapped region includes the incoming beam, the wedge and the emerging refracted beam. While both the intensity [Fig. 4(a)] and real part of the field [Fig. 4(b)] indicate the expected positive bending of the beam, there is a considerable amount of scattering of the wave within the wedge. In prior refraction experiments and simulations, the multiple scattering associated with a narrow beam within a wedge has been suggested as the cause of multiple observed refracted beams [25]. The lack of coherent phase fronts within the sample in the map of the real part of the field provides further evidence that considerable multiple scattering occurs.

Previous analysis has suggested that illumination by a broad beam, on the order of the wedge base, can lessen the multiple scattering and lead to a more coherent phase within the

#73265 - $15.00 USD Received 21 July 2006; revised 6 September 2006; accepted 6 September 2006

sample [26]. The influence of the aperture on the internal field of the wedge was tested by illuminating the prism with a broad beam, as shown in Fig. 4(c), which shows the measured real part of the electric field. Indeed, the phase fronts within the wedge are seen to be considerably more coherent.

It is interesting to note the differences in the information available from the intensity versus the real field plots. The intensity maps of the squared value of the electric field, $E_r(x,y)^2 + E_i(x,y)^2$, provide an indication of where the energy is located within the scattering region, and also reveal the location of standing waves. As can be seen from Fig. 4(a), there is a substantial amount of reflection at the wedge interfaces, leading to a complicated standing wave pattern within the wedge, as well as a significant standing wave component at the input to the wedge. It appears also that the multiple reflected beams within the wedge lead to additional refracted beams, as can be seen near the upper right corner of the wedge. In contrast, the real part of the electric field [Fig. 4(b)] shows clearly the refraction properties of the main beam as it exits the wedge as well as the propagation fronts as the wave passes through the wedge. In addition, the reduced wavelength within the wedge can be seen by noting the distance between the nodes of the phase fronts and comparing with the field outside the wedge. Animations of the real field show that the phase fronts advance away from the source (i.e., from the bottom to the top of the figure).

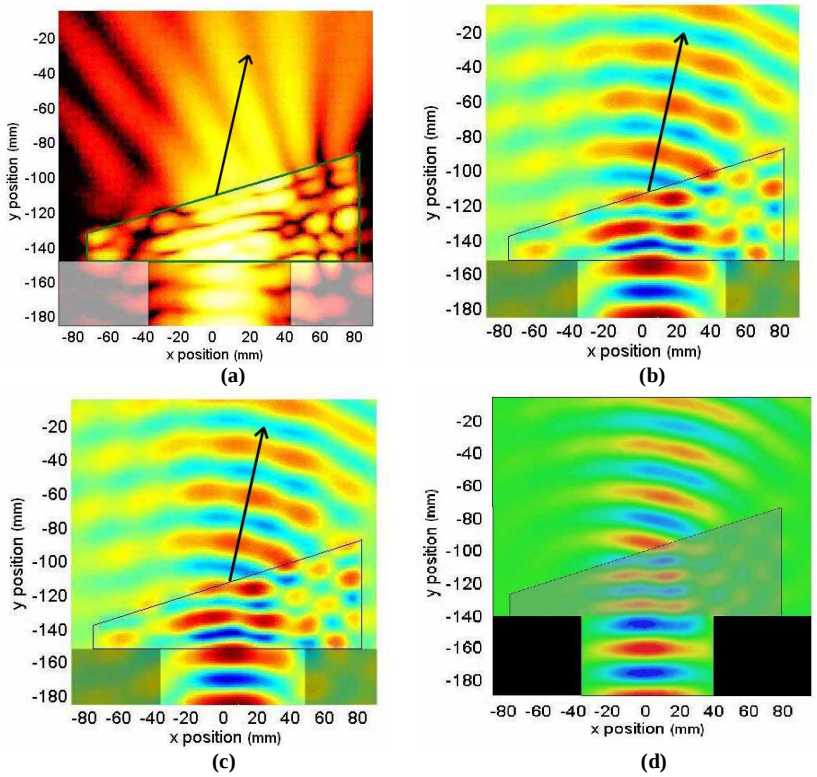

Fig. 4. A microwave beam refracting from a positive index (polycarbonate, ε=2.6) wedge at 10.5 GHz. (a) Measured spatial map of the electric field intensity with an arrow indicating expected angle of refraction. (b) (1.65 MB) Measured spatial map of the real part of the electric field. (c) (1.69 MB) Measured spatial map of the real part of the electric field, with a larger input aperture. (d) (0.84 MB) Numerical simulation of a positive index wedge with the same parameters as in (c).

#73265 - $15.00 USD Received 21 July 2006; revised 6 September 2006; accepted 6 September 2006

4. Negative index metamaterial wedge experiments

All known, naturally occurring, transparent materials possess a positive index of refraction. It is possible, however, to create a metamaterial having a *negative* index of refraction by designing an artificial structure with permittivity and permeability both less than zero [27]. The details of this design procedure are not of direct importance here, and we refer the reader to the extensive prior work contained in the references above [2-17]. In the present case, we desired to produce a sample having a negative index of refraction over a band of microwave frequencies that would be compatible with our planar waveguide apparatus. The resulting design is presented in Fig. 5, which shows diagrams of the unit cells as well as a photograph of the assembled wedge sample.

One of the important design features of the metamaterial shown is the "I-beam" structure of the wire elements that give rise to the negative permittivity response. Because the upper and lower plates are moved relative to each other, it is not possible to create a wire structure having electrical continuity between the upper and lower plates. The frequency-dependent electric permittivity for a continuous wire medium has a simple Drude form. The permittivity for wire medium that does not have electrical continuity has a resonant Drude-Lorentz form, with the resonant frequency strongly dependent on the capacitance between the ends of the wires and the bounding conducting plates. The dependence on this capacitance causes the effective medium properties of the metamaterial sample to be extremely sensitive to the gap between the bounding plates and the metamaterial; for some designs, differences of just a few microns can mean the difference between a metamaterial with positive or negative permittivity [10]. After simulating numerous wire lattice designs, performed using the commercial finite-element code HFSS (Ansoft), we determined that the change in permittivity of the I-beam wire lattice, shown in Fig. 5, was relatively insensitive to the likely errors in plate separation. That is, the expected permittivity is always negative for this structure given the tolerances associated with the planar waveguide apparatus.

ε	-0.85+0.105*i*
μ	-0.53+0.108*i*
n	-0.67+0.110*i*
Z	0.79-0.032*i*

(a)

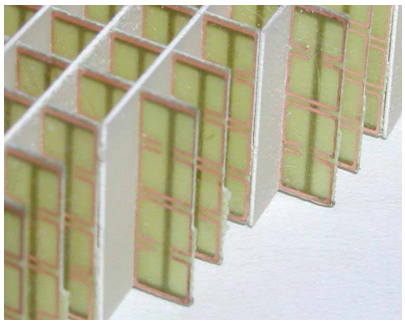

(b)

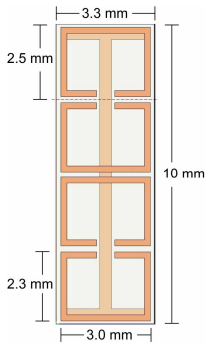

(c)

Fig. 5. Design of the negative index metamaterial. (a) Extracted parameter set from the simulation of a single unit cell at 10.5 GHz. (b) A photograph of the fabricated wedge, showing the elements and construction near the angled surface. (c) A planar view of the unit cell, with dimensions indicated. The gap in the rings is 0.6 mm, while the line width is 0.2 mm. The wire, patterned on the reverse side of the circuit board, has a length of 9.8 mm (including the cross pieces), with a line width of 0.4 mm. The cross pieces extend a length of 3.0 mm. The circuit board material (FR4) has a thickness of 0.20 mm, with a dielectric constant of 3.71. The copper thickness for all structures is 17 μm.

#73265 - $15.00 USD Received 21 July 2006; revised 6 September 2006; accepted 6 September 2006

After the appropriate design was determined, a wedge was fabricated from the metamaterial utilizing standard lithographic techniques as previously reported [28]. Rather than being isotropic in the plane of propagation, the assembled sample is anisotropic, such that the permeability is only negative along one dimension of the medium (although the permittivity is negative for all wave propagation directions within the plane). The underlying medium is therefore *indefinite*, in that the permeability tensor has both positive and negative diagonal elements. While perhaps not immediately evident, a wedge formed of an indefinite medium behaves in the same manner as a wedge made of isotropic negative index material, as has been discussed previously [25], so long as the incident wave is of the correct polarization and is incident along a principle axis of the medium.

The results of the negative index metamaterial wedge experiment are presented in Fig. 6. The incident beam is channeled through the absorber to be incident on one face of the wedge at normal incidence. The frequency of operation for the prism was 10.5 GHz, the same frequency at which the polycarbonate prism was mapped. As both the intensity [Fig. 6(a)] and real field [Fig. 6(b)] maps show, the wave propagates through the metamaterial and is subsequently refracted at the second interface. The second interface is sloped at an average angle of 18.4º, as set by the 3:1 stepping of the unit cells (indicated by the outlines in Fig. 6). Because the FR4 is a relatively lossy substrate material, significant absorption of the wave occurs through the sample; to obtain the best results, only the leftmost portion of the sample is illuminated to minimize the absorption of the wave as it travels through the structure. No attempt was made here to quantify the observed refraction properties with those predicted from the design simulations. Given the ambiguity of the plate separation, it is difficult to obtain an exact match in frequency and other characteristics between the simulations and the measurements. Clearly, the wave that emerges from the oblique face is negatively refracted, in qualitative agreement with the simulated negative index frequency band. A survey over all other frequencies in the acquisition range (8-12 GHz) confirmed that the observed negative refraction occurred only over a narrow frequency range centered at 10.5 GHz, consistent also with the unit cell simulations.

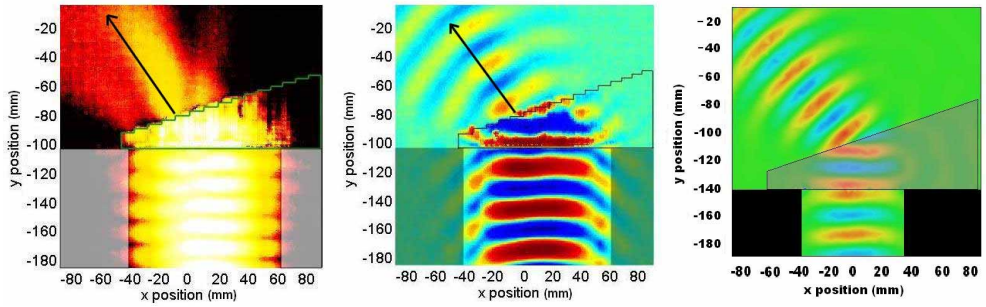

Fig. 6. (a). Measured spatial map of the intensity of a beam refracting from the negative index metamaterial sample at 10.5 GHz. The arrow indicates the expected angle of refraction as extracted from the unit cell simulations. (b) (1.53 MB) Measured spatial map of the real part of the electric field for the same configuration. (c) (0.77 MB) Numerical simulation of a negative index wedge at the same frequency.

The field maps of the real part of the field are particularly striking within the region of the metamaterial, in that the phase fronts [Fig. 6(b)] appear nearly uniform as would be expected for a homogeneous material. Even more remarkably, the animation of the real field shows that the phase fronts progress "backwards" within the wedge sample, away from the refraction interface and towards the first interface. (Note that the stepping of the refraction interface is drawn as smooth on the animation for this and subsequent samples). This reversal of phase

#73265 - $15.00 USD Received 21 July 2006; revised 6 September 2006; accepted 6 September 2006

and energy velocities is one of the key signatures of a negative index medium [27], and is further consistent with the observed refraction. The underlying metamaterial structure, while subtle, can be seen as the pixilation, or slight modulation in the field amplitude, corresponding to the unit cell dimension (3 mm). Figure 6(b) thus provides information on both the homogeneous metamaterial approximation and the actual inhomogeneous, discrete lattice structure. Even the resulting grating of the refraction interface—the stepped surface in the figures—does not appear to introduce noticeable artifacts into the scattered field.

The plots of the real field are particularly convenient for comparison with numerical simulations on homogeneous structures. For comparison, we have included the results of numerical simulations for both the positive index [Fig. 4(d)] and the negative index [Fig. 6(c)] wedges. The simulations were performed in HFSS utilizing the same technique previously reported [28]. For the simulations, a homogeneous negative index wedge is placed between a pair of perfect electric walls that constrain the electromagnetic field in the same way as the conducting plates of the experimental apparatus. It should be noted, however, that the top of the wedge touches the upper perfect electric wall in the simulation, which is in contrast to the case of the mapping chamber where a small gap allows the displacement of the wedge with respect to the probing antenna. The calculation domain is otherwise terminated by radiation boundaries that fully absorb waves impinging upon them. An input port is used to source the electromagnetic wave into the computational domain, while a set of radiation boundaries play a role similar to that of the absorber used in the experiments to channel the incident beam towards the wedge. On the exit side, the use of radiation boundaries prevents the waves from being reflected at the edges of the computational domain, thus suppressing numerical artifacts due to the finite size of the model. Figures 4(d) and 6(c) show the real part of the electric field when the permittivity of the wedge is +2.6 and -1.4, respectively. The overall agreement with the actual measured structures is excellent in both cases, although the measured phase fronts are somewhat less planar in the experiments than those in the simulations. This deviation from the ideal is not unexpected, as the fabrication tolerances likely lead to some spread in the local electromagnetic properties.

That the wave fronts are perturbed very little by the discrete nature of the wedge sample provides further support that metamaterial structures can be treated as homogeneous media with effective optical properties. However, as discussed above, the fields are probed not inside the wedge but rather just above the sample. As a result, the continuous wave fronts of Fig. 6 could possibly represent an artifact of the experiment, if the fields detected by the antenna differ significantly from those inside the metamaterial structure. In order to dismiss this latter possibility, we intentionally introduce a local defect inside the metamaterial by removing a cluster of six unit cells (2 x 3 unit cells) in the center of the prism, then repeated the experiment. Spatial maps of the intensity and the real part of the electric field for the wedge with defect are presented in Figs. 7(a) and 7(b). The region of the defect is indicated by a rectangular overlay within the wedge. Both the fields inside the wedge and the refracted beam are affected by the defect: the wavefronts within the wedge are no longer continuous and the refracted beam is split into three lobes.

It is not immediately clear from Figs. 7(a) and 7(b) whether the defect has caused the effective medium description to breakdown, or if all of the observed scattering within and outside of the wedge can be described by a homogeneous negative index wedge with a defect. To test the latter, we simulated a wedge with an air defect matching the dimensions and other parameters used in the measurement. From the computed map of the real part of the electric field, shown in Fig. 7(c), we find that the field for a homogeneous wedge with a defect matches fairly well the actual measured field of the metamaterial sample. In particular, three well-defined beams are seen emerging from the wedge, as observed in the experiment. The result illustrates that metamaterials of arbitrary shape and morphology can still be described as being composed of homogeneous material. This conclusion is consistent with the observation of enhanced diffraction in far-field measurements, in which the stepping of the wedge surface due to the finite unit cell size gives rise to a first order diffracted beam [30].

#73265 - $15.00 USD Received 21 July 2006; revised 6 September 2006; accepted 6 September 2006

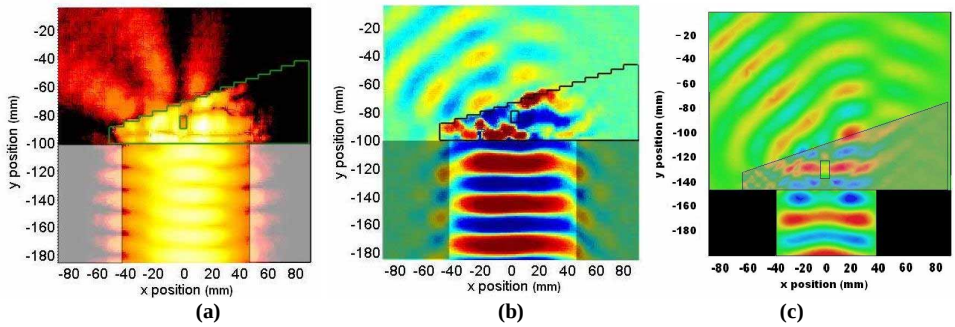

Fig. 7. (a). Measured spatial map of the intensity of the beam refracting from the negative index metamaterial sample with a small local structural defect introduced, causing corruption of the refracted beam at 10.5 GHz. (b) (1.63 MB) Measured spatial map of the real part of the electric field for the same configuration, with defect. Note that the phase fronts within the negative index wedge are no longer uniform. (c) (0.87 MB) Numerical simulation of a homogeneous negative index wedge with defect.

5. Conclusion

We have demonstrated that it is feasible to measure directly the fields internal and external to inhomogeneous two-dimensional metamaterial samples. Remarkably, we find that the homogeneous description of the metamaterial can be directly confirmed by the presence of "macroscopic" uniform phase fronts that coincide extremely well with simulations in which the metamaterial structures are replaced with homogeneous materials. The results, consistent with previous work, illustrate the validity and utility of the metamaterials concept. The phase fronts measured from the actual samples display an increased amount of distortion when compared with the simulations, but this can be understood by local imperfections introduced during fabrication that produce an index that varies spatially within some range. Presumably, this effect could be included in the simulations to achieve even closer agreement. Conversely, the field maps could be used to identify local regions in fabricated samples whose properties deviate from the expected. While a visual inspection of the samples used here would probably reveal the non-uniform regions, other types of metamaterial samples are less amenable to non-destructive evaluation [17]. For complex metamaterial samples with spatial gradients in one or more of the electromagnetic parameters, the field mapping may prove an invaluable tool for confirming the anticipated scattering behavior.

Acknowledgments

This work was supported by Multidisciplinary University Research Initiatives, sponsored by DARPA/ONR (Grant No. N00014-01-1-0803). D. Schurig acknowledges support from the IC Postdoctoral Fellowship Program.

#73265 - $15.00 USD Received 21 July 2006; revised 6 September 2006; accepted 6 September 2006